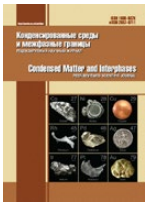

ISSN 1606-867X (Print)
ISSN 2687-0711 (Online)
Condensed Matter and Interphases
Kondensirovannye Sredy i Mezhfaznye Granitsy
https://journals.vsu.ru/kcmf/

Original articles

Research article
https://doi.org/10.17308/kcmf.2025.27/13022

Double borate $NaScB_2O_5$: synthesis, thermal stability, ionic conductivity, IR spectroscopy, and electronic structure

A. N. Sobolev[1,2], E. V. Kovtunets[1,2], T. S. Spiridonova[1,2], A. B. Bogdanov[3], A. K. Subanakov[1,2]✉

[1]Baikal Institute of Nature Management, Siberian branch of the Russian Academy of Sciences
6 Sakhyanovoy st., Ulan-Ude 670047, Russian Federation

[2]Banzarov Buryat State University,
24a Smolina st., Ulan-Ude 670000, Russian Federation

[3]Vinogradov Institute of Geochemistry, Siberian branch of the Russian Academy of Sciences
1a building, Favorskogo st., Irkutsk 664033, Russian Federation

Abstract

Objective: Sodium scandium double borate ($NaScB_2O_5$), whose crystal structure was solved by Backer and Held in 2001, remains a poorly explored compound. The crystal structure has wide channels that may suggest the ionic conduction of sodium ions. Based on this, the aim of the study was to investigate the ionic conductivity of this compound, as well as to study its thermal behavior, measure the IR spectrum, and calculate the electronic structure by quantum chemical method.

Experimental: The synthesis of sodium scandium double borate ($NaScB_2O_5$), was achieved using a solid-state reaction method. $NaScB_2O_5$ was explored by using thermal analysis, IR spectroscopy, ionic conductivity, theoretical estimates of activation energy, ion transport pathways, and ab initio calculations of the electronic structure.

Conclusions: Rietveld method was engaged: monoclinic symmetry (sp. gr. $P2_1/c$), a = 7.2460(2) Å, b = 9.7887(3) Å, c = 5.9289(2) Å, β = 71.318(1) °, Z = 4, V = 398.37(2) Å^3, R_{wp} = 2.81, GOF = 1.64. $NaScB_2O_5$ borate is characterized by incongruent melting at 1090 °C. The calculated ab initio IR spectrum of $NaScB_2O_5$ exhibited a high degree of consistency with the experimentally obtained IR spectrum. The calculated energy barrier for oxygen ion migration, determined to be 0.998 eV, exhibits a reasonable degree of agreement with the experimentally determined activation energy of 0.9 eV. The title compound exhibits an ionic conductivity of $0.6 \cdot 10^{-3}$ S/cm at 1023 K. The band gap was about 6.83 eV.

Keywords: Sodium scandium borate; Solid-phase synthesis; Thermal analysis; IR spectroscopy; Electrical conductivity

Funding: The work was supported by a grant from the Russian Science Foundation (No. 23-23-00451) and partially with the financial support of the Ministry of Science and Higher Education of the Russian Federation (State assignment of the BIP SB RAS No. 0273-2021-0008)."

Acknowledgments: The authors express their gratitude to Dr. R. Yu. Shendrik for help with the ArDI web application. The studies by XRD, thermal analysis, FT-IR spectroscopy and conductivity were carried out using the resources of the Center for Collective Use of BIP SB RAS. Ab initio calculations were performed on the «Academician V. M. Matrosov» complex of the Irkutsk Supercomputer Center of the Siberian Branch of the Russian Academy of Sciences [https://hpc.icc.ru/].

For citation: Sobolev A. N., Kovtunets E. V., Spiridonova T. S., Bogdanov A. I., Subanakov A. K. Double borate $NaScB_2O_5$: synthesis, thermal stability, ionic conductivity, IR spectroscopy, and electronic structure. *Condensed Matter and Interphases*. 2025;27(3): 454–463. https://doi.org/10.17308/kcmf.2025.27/13022

Для цитирования: Соболев А. Н., Ковтунец Е. В., Спиридонова Т. С., Богданов А. И., Субанаков А. К. Двойной борат $NaScB_2O_5$: синтез, термическое поведение, электропроводность и электронная структура. Конденсированные среды и межфазные границы. 2025;27(3): 454–463. https://doi.org/10.17308/kcmf.2025.27/13022

✉ Alexey K. Subanakov, subanakov@binm.bscnet.ru

1. Introduction

Borates have a unique set of physicochemical properties, which determines their significant potential for research in various fields. They are excellent starting materials for optical applications. Due to their crystallographic diversity, wide range of optical transparency, and unique properties, borates have been widely recognized as nonlinear optical materials in the ultraviolet (UV) and deep UV region [1–7]. The following nonlinear optical crystals are currently used commercially: β-BaB_2O_4 [8] and LiB_3O_5 [9]. In addition to the above, the following nonlinear optical crystals are of particular interest to materials scientists: $CsLiB_6O_{12}$ [10], $KBe_2B_2O_3F_2$ [11], $Sr_2Be_2B_2F_7$ [12], and BiB_3O_6 [13]. Centrosymmetric borates such as α-BaB_2O_4 [14], $Ca_3(BO_3)_2$ [15], $Ba_3YB_9O_{18}$ [16], $Ca(BO_2)_2$ [17] having high birefringence are promising materials for light polarization in the deep-UV range of the spectrum.

Pyroborates containing the $[B_2O_5]^{4-}$ anionic group were first structurally characterized in 1950. [18]. Pyroborates can be divided into two classes: alkaline-earth pyroborates $A_2B_2O_5$ (A = Mg, Ca, Sr (alkaline-earth metals)) [19], $Li_{3.366}Mg_{0.317}B_2O_5$ [20], $BaMnB_2O_5$ [21], and transition metal pyroborates $MM'B_2O_5$: $Co_{2-x}Ni_xB_2O_5$ [22], $Ni_{1.5}Zn_{0.5}B_2O_5$ [23], $Co_{1.5}Zn_{0.5}B_2O_5$ [23]. In addition, there are pyroborates of alkali $Li_2PbB_2O_5$ [24] and rare earth metals $Pr_2(B_2O_5)(MoO_4)$ [25]. Borates containing pyroborate group – $[B_2O_5]^{4-}$ can be considered as one of the most promising for light birefringence in the deep UV range [26]. For high birefringence it is necessary that borate triangles in the $[B_2O_5]^{4-}$ group are coplanar, i.e. lie in the same plane.

Our scientific interest was attracted by sodium scandium double pyroborate ($NaScB_2O_5$) [27], the crystal structure of which is solved on single crystals, but the other properties and characteristics have not been investigated. For light polarization (birefringence) problems, this double borate is not suitable because the torsional angle between the planes of borate triangles is about 30°, which is unacceptable for significant birefringence. The presence of channels in the crystal structure of this borate implies high ionic conductivity. Therefore, the aim of the present work was to study the ionic conductivity of this compound, as well as to study its thermal behavior, characterize it by IR spectroscopy and calculate its electronic structure by a quantum chemical method.

2. Experimental

For solid-phase synthesis of double borate, the following reagents were used: Na_2CO_3 (h.p.), Sc_2O_3 (h.p.), H_3BO_3 (h.p.). Prior to synthesis, the carbonate and oxide were annealed at 500 °C for 8 h to remove extracted moisture. The reaction mixture of the starting components Na_2CO_3, Sc_2O_3, and H_3BO_3 in the ratio of 1:1:4, respectively, was homogenized in an agate mortar and annealed at 300 °C (heating rate 1 °C/min) for 24 h in a muffle furnace to remove volatile reaction products: CO_2 and H_2O. After annealing, the reaction mixture was homogenized and annealed at 500 °C for 24 h, followed by X-ray diffraction analysis (XRD) of the mixture. Further, stepwise annealing was carried out at 500-600 °C for 5 h and finally at 750–800 °C for 20 h with intermediate grindings until equilibrium was reached. The single-phase nature of the reaction product and the achievement of equilibrium were monitored by XRD.

D8 ADVANCE (Bruker AXS) and DM-20 (TONGDA) diffractometers with CuKα-radiation were used for XRD. The following imaging conditions were used: Bragg–Brentano geometry, scanning range from 8 to 80° by 2Θ with a step of 0.02°, room temperature.

Rietveld refinement [28] was performed using the TOPAS 4.2 [29, 30] software suite.

An STA 449 F1 Jupiter thermal analyser (NETZSCH) was used for thermogravimetric (TG) and differential scanning calorimetric (DSC) characterization of the title compound. The thermal analysis was carried out in the temperature range of 200–1200 °C in an argon flow at a rate of 10 °C/min, using platinum crucibles. The use of Pt–PtRh thermocouple increased the accuracy of temperature measurement to ±1°.

The theoretical evaluation of activation energy and ion transport pathways was carried out by the SoftBV program [31]computational tools are sought to accelerate materials discovery by computational predictions. Here are introduced a set of computationally inexpensive software tools that exploit the bond-valence-based empirical force field previously developed by the authors to enable high-throughput computational screening of experimental or simulated crystal-structure models of battery materials predicting a variety of

properties of technological relevance, including a structure plausibility check, surface energies, an inventory of equilibrium and interstitial sites, the topology of ion-migration paths in between those sites, the respective migration barriers and the site-specific attempt frequencies. All of these can be predicted from CIF files of structure models at a minute fraction of the computational cost of density functional theory (DFT using bond valence sum maps (BVS).

For studying the electrical conductivity, the ceramic disks of $NaScB_2O_5$ (∅ = 10 mm, h = 1.6 mm) were prepared by pressing the powder at 1 kbar and sintering at 1073 K for 4 h. For preparing the electrode, the disk surface was coated with colloidal platinum, followed by annealing for 1 h. The electrical conductivity was measured by the two-contact method (impedance meter Z-1500J, frequency range 1 Hz – 1 MHz, temperature range of 473–1023 K, heating and cooling rates of 2 K/min). The activation energy values were calculated from the slope of the straight lines corresponding to the Arrhenius dependence in $\lg(\sigma T) - (10^3/T)$ coordinates.

Ab initio calculations were performed using the VASP software package [32] based on density functional theory (DFT). A pseudopotential approach with basis functions in the form of plane waves was used in the calculations. The kinetic energy limit is 400 eV. A 2 × 1 × 2 grid of wave vectors centered at the Γ point was used for integration over the Brillouin zone. The positions of the atoms were displaced by the relaxation of the cell with a force of no more than 0.001 eV/Å. The Perdew–Burke–Ernzerhof exchange-correlation functional (PBESol) [33] was used to calculate the electronic structure of $NaScB_2O_5$. The IR spectrum was calculated in VASP using the procedures included in the Phonopy code [34]. The HSE06 hybrid functional [35] was used to calculate the electronic density states. The graph of electronic density states was generated in [https://github.com/QijingZheng/pyband].

Table 1. $NaScB_2O_5$ unit cell parameters in comparison with [27]

Sp. Gr.	monoclinic $P2_1/c$ [in this work]	monoclinic $P2_1/c$ [27]
a, Å	7.2460(2)	7.2339(6)
b, Å	9.7887(3)	9.7966(6)
c, Å	5.9289(2)	5.9233(5)
α, °	90	90
β, °	71.318(1)	71.483(8)
γ, °	90	90
V, $Å_3$	398.37(2)	398.0

3. Results and discussion

3.1. Crystal structure

The Rietveld method was applied to identify the target phase and its purity. The crystal structure of ScB_2O_5 is known and described in [27], the positions of atoms and their displacements were not specified. All reflexes in the diffractogram were assigned to the monoclinic sodium scandium double borate $NaScB_2O_5$ (pr. gr. $P2_1/c$) [27] with low unreliability factors: R_{wp} = 2.81 %, R_p = 2.12 %, R_{exp} = 1.71 %, χ^2 = 1.64, R_B = 1.59 %. Figure 1 shows the experimental, calculated, and difference diffractograms of $NaScB_2O_5$. The parameters of the $NaScB_2O_5$ unit cell were refined in this work in comparison with the data of [27] are presented in Table 1.

The crystal structure of $NaScB_2O_5$ (Fig. 2a) consists of slightly distorted octahedrons [ScO_6], which form zigzag chains along the "c" axis, connecting through common edges. These chains are joined together through pyroborate groups [B_2O_5] and distorted tetrahedra [NaO_4]. Each pyroborate group is connected to five [ScO_6] octahedra and three [NaO_4] tetrahedra. The pyroborate group consists of two planar triangles [BO_3] joined through a common oxygen vertex with a rotation angle of about 40°. Figure 2b illustrates a projection onto the (20) plane showing the "wide

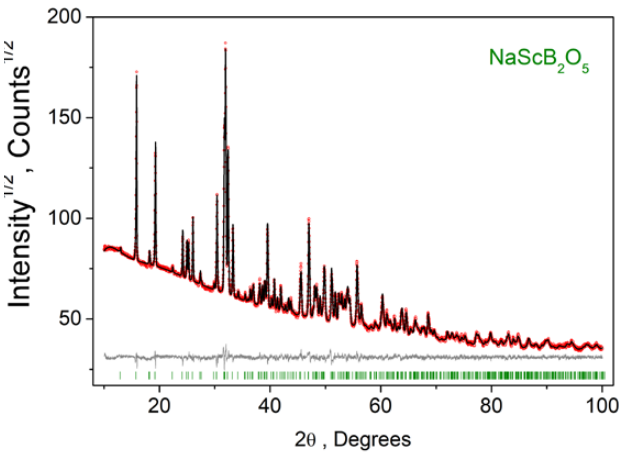

Fig. 1. Rietveld plot of $NaScB_2O_5$ – experimental (red), calculated (black), difference (grey), reflections (green)

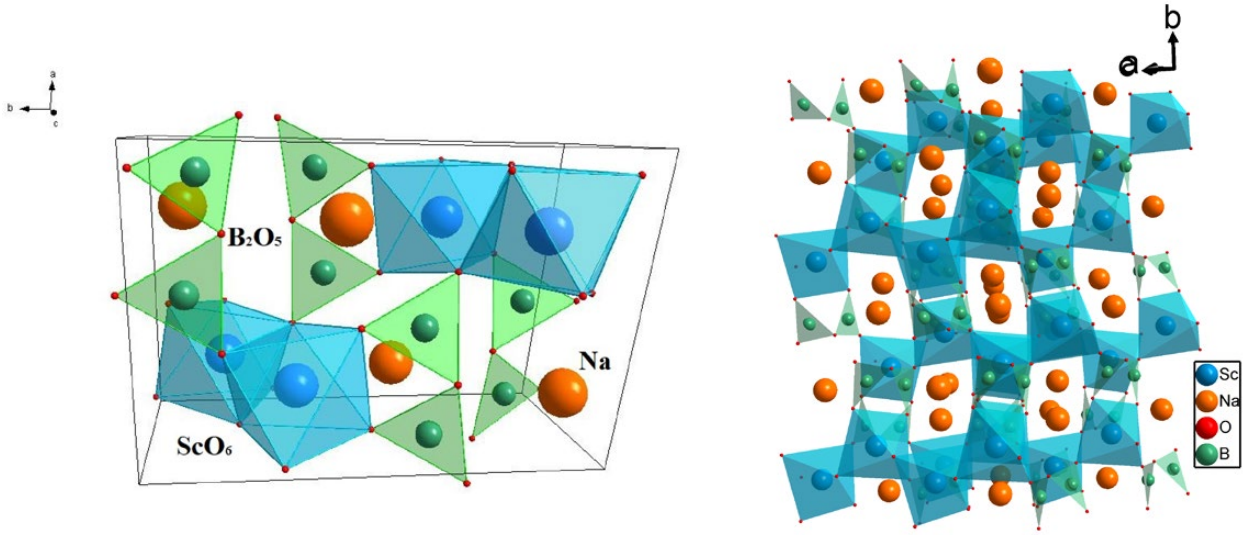

Fig. 2. Crystal structure of $NaScB_2O_5$ (a); b – crystal structure projection of $NaScB_2O_5$ onto the ((20$\bar{1}$)) plane (b)

channels" filled with sodium cations. The crystal structure of $NaScB_2O_5$ was constructed according to the data [27] in the Diamond 3.2 program.

3.2. Thermal properties

Fig. 3 shows the heating and cooling curves of $NaScB_2O_5$ in the temperature range from 200 to 1200 °C. The endothermic effect at 1090 °C corresponds to the melting temperature of the double borate. Three endotherms corresponding to the crystallization of $NaScB_2O_5$ decomposition products are observed on the DSC cooling curve, which can be considered as an indirect confirmation of the incogruent melting of this borate. The diffractogram of $NaScB_2O_5$ after melting is presented in the supplementary materials (S1), which shows the reflexes of the following compounds: $ScBO_3$ [01-079-0097], Sc_2O_3 [00-005-0629], and $Na_2Al_2B_2O_7$ [00-053-1124]. The melting of $NaScB_2O_5$ for XRD was carried out in a corundum (Al_2O_3) crucible, which caused the interaction of the borate melt with the crucible material, so the diffractogram showed reflections of double aluminum and sodium borate ($Na_2Al_2B_2O_7$). XRD results of samples annealed at temperatures (700, 750, 800, 850, 900, 950 °C) showed the presence of the $NaScB_2O_5$ phase only, which indicates the thermal stability of $NaScB_2O_5$ at these temperatures.

3.3. Conductivity measurements

3.3.1. The theoretical evaluation of activation energy and ion transport pathways

Potential barriers and ionic transport pathways of sodium and oxygen were evaluated

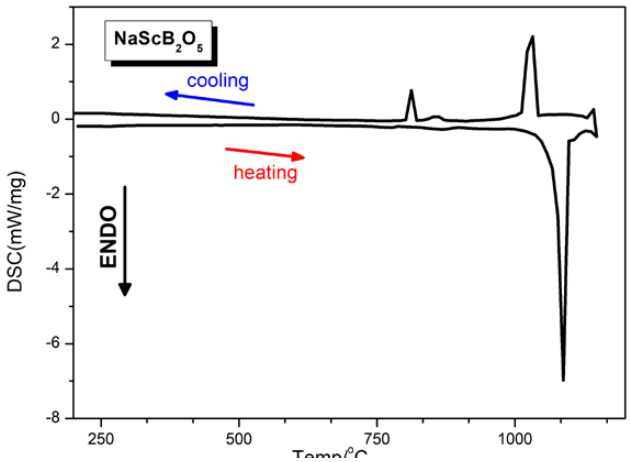

Fig. 3. DSC curve recorded for $NaScB_2O_5$

using valence force sum maps. According to calculations, the total electrical conductivity of $NaScB_2O_5$ may include contributions of both sodium and oxygen ions (Table 2), indicating the three-dimensional conductivity of these ions in the crystal structure of the studied borate. However, the barrier of two-dimensional conductivity of sodium (0.936 eV) is comparable to the energy barrier of three-dimensional conductivity of oxygen (0.998 eV), while the analogous one for sodium ions is much lower (1.246 eV). The energy profile along the sodium ion pathway is shown in Fig. 4, and the calculated isosurfaces of the energy barriers of sodium and oxygen ions are shown in Figs. 5 and 6.

Table 2. Calculated energy barrier values of testing ions in $NaScB_2O_5$

Testing ions	Energy barrier, eV	Dimension of conductivity
Na^+	0.856	1D [0,0,1]
	0.936	2D (1,0,0)
	1.246	3D
O^{2-}	0.629	1D [1,0,–1]
	0.998	3D

3.3.2. Experimental measurements of the electrical conductivity

The temperature dependence of the electrical conductivity is presented in Fig. 7 in Arrhenius coordinates. The dependence obtained is close to linear. The conductivity varies from $0.6 \cdot 10^{-7}$ S/cm (300 °C, E_a = 0.7 eV) to $0.6 \cdot 10^{-3}$ S/cm (750 °C, E_a = 0.9 eV). Figure 8 shows the impedance spectra of the double borate. The obtained Z′(Z″)

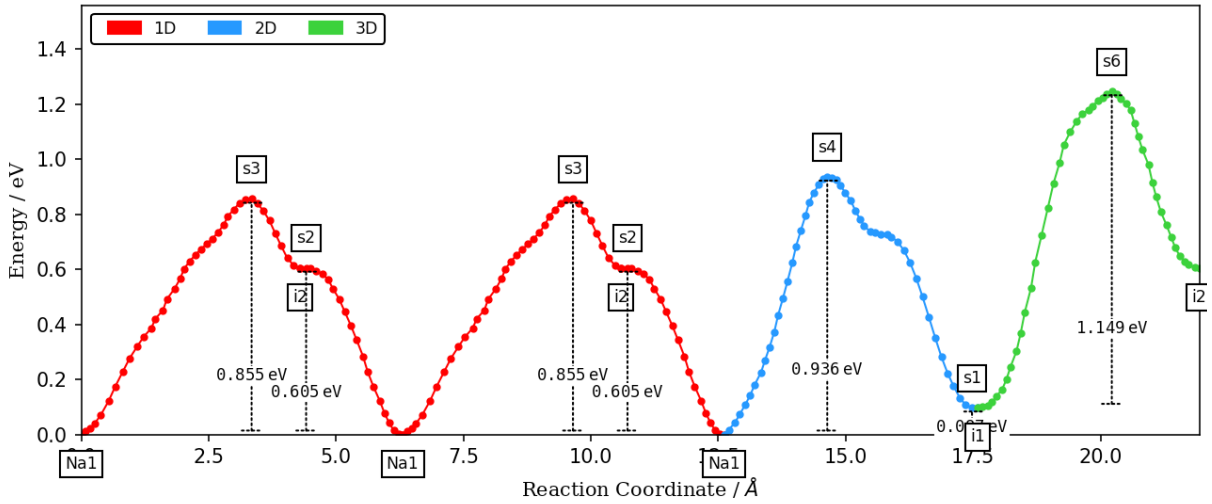

Fig. 4. Energy profile along the route of sodium transport in the $NaScB_2O_5$ structure

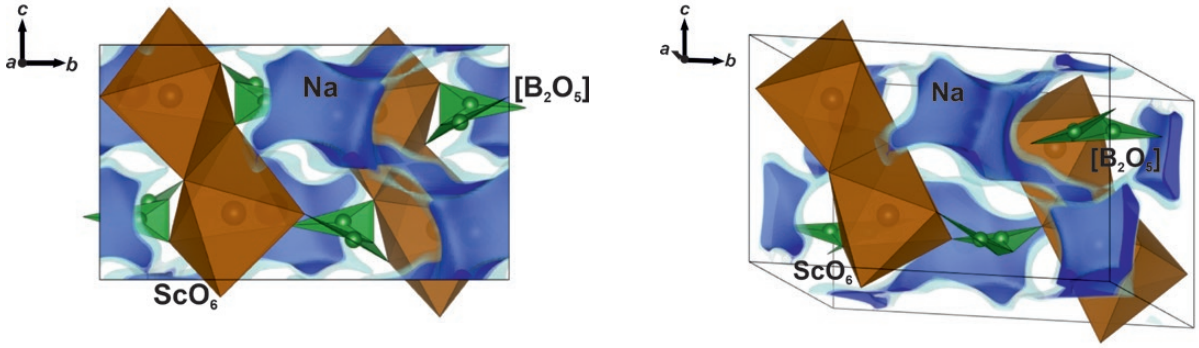

Fig. 5. Calculated isosurfaces of activation energies of sodium ion transport in the $NaScB_2O_5$ structure

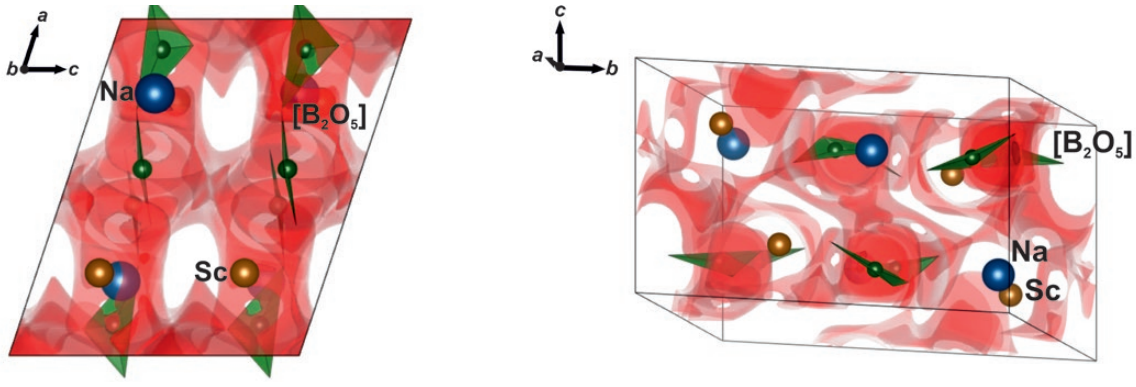

Fig. 6. Calculated isosurfaces of activation energies of oxygen ion transport in the $NaScB_2O_5$ structure

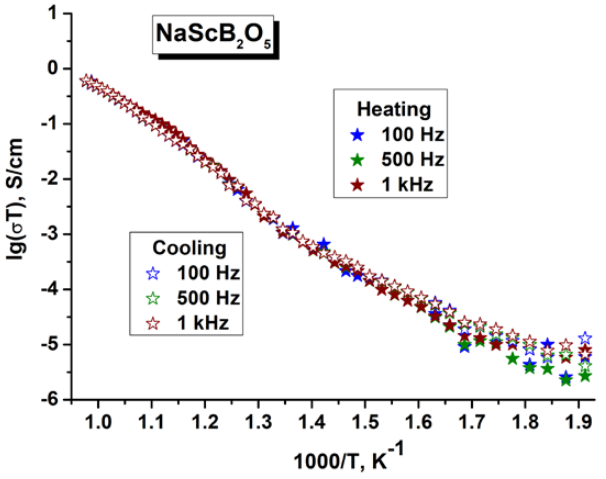

Fig. 7. Temperature dependences of electrical conductivity for $NaScB_2O_5$

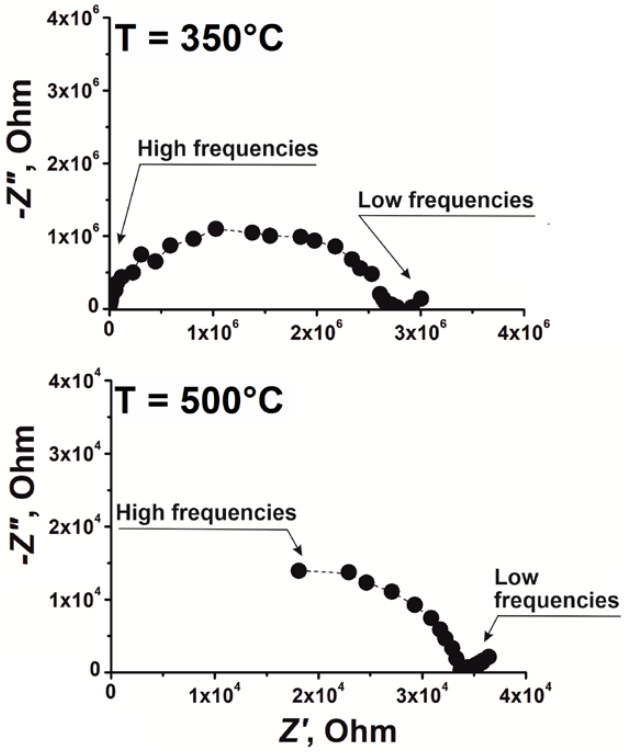

Fig. 8. The impedance profiles for $NaScB_2O_5$ borate measured at different temperatures

interdependence is typical for ionic conductors with blocking electrodes; the line in the low-frequency region corresponding to the ion transport blocking electrodes also indicates the ionic character of the conductivity.

3.4. Infrared spectra

The IR spectrum of sodium scandium borate was measured to compare with the spectra of

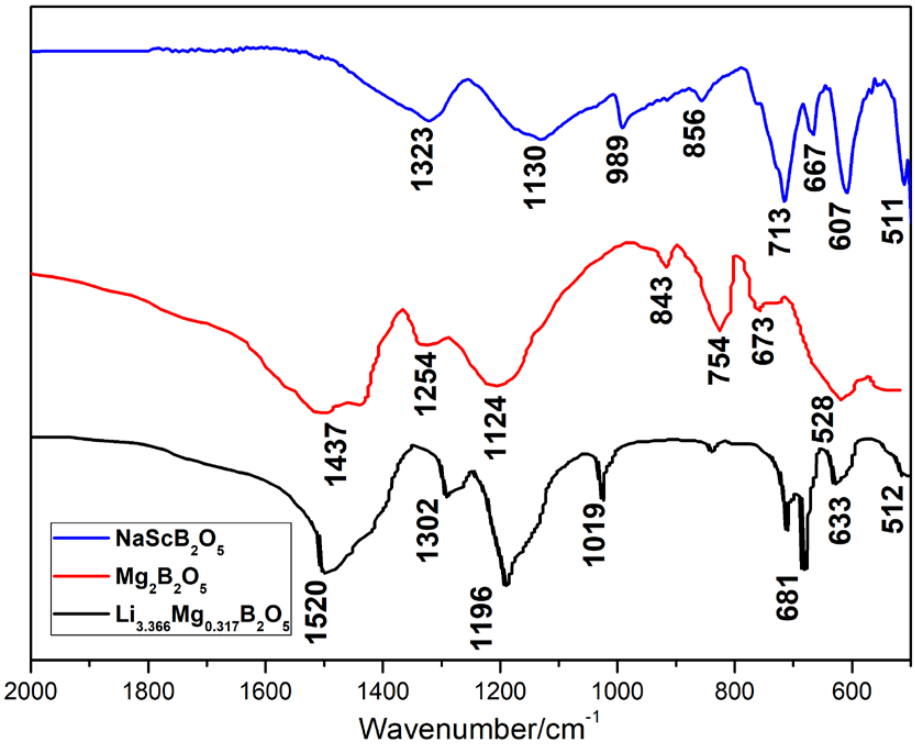

Fig. 9. The infrared spectra of $NaScB_2O_5$, $Mg_2B_2O_5$ and $Li_{3.366}Mg_{0.317}B_2O_5$ [20]

known pyroborates and the IR spectrum of $NaScB_2O_5$ calculated by the ab initio method. The band at 1323 cm^{-1} refers to the antisymmetric valence vibrations of the BO_3 group, whereas the bands at 1130, 989 and 856 cm^{-1} refer to the symmetric valence vibrations of the B – O bonds in the BO_3 group. The bands at about 713, 667, 607 cm^{-1} belong to out-of-plane strain vibrations of the BO_3 group, and the band at 511 cm^{-1} to in-plane strain vibrations. Thus, the IR spectra further confirmed the triangular coordination of boron found from the crystal structure solution of $NaScB_2O_5$. In addition, the obtained IR spectrum of $NaScB_2O_5$ was compared with the IR spectra of minerals using the ArDI Internet application (https://ardi.fmm.ru/) [36]. As a result of the search, the following minerals with similar IR spectra were found: Suanite, Shimazakiyite_B117, Clinocurcate_B3, and Curcate_B36_B36 (S2). All the above minerals belong to borates with the B_2O_5 pyrogroup. Additionally, the IR spectrum of $NaScB_2O_5$ was calculated by the ab initio method. The comparison showed a relatively good match between the position of the absorption peaks of the calculated spectrum and the experimental spectrum (Fig. 10). As can be seen from Fig. 10, there is a difference in the intensities of the calculated and experimental spectra. The discrepancy in the intensities between the calculated and experimental IR spectra, in our opinion, is caused, firstly, by the use of the harmonic approximation in the calculation, and secondly, by the neglect of temperature effects, since the calculation technique implies calculation at absolute zero. Nevertheless, the figure shows a good match between the calculated and measured peak positions, which allowed us to interpret the nature of the oscillations.

3.5. Electronic structure

The $NaScB_2O_5$ crystal lattice underwent relaxation to the total energy minimum. The crystal structure of $NaScB_2O_5$ was optimized with the PBEsol functional. The lattice vectors were fixed at values determined experimentally, and the atomic positions were relaxed until the maximum component of the forces acting on the atoms was less than 0.001 eV/Å. After relaxation of the geometry, the volume of the unit cell did not change, but the atoms were significantly displaced from their original positions. The maximum displacements of Na atoms were 0.062 Å, Sc atoms were 0.016 Å, B atoms were 0.032 Å, and O atoms were 0.054 Å. Then, using the optimized crystal lattice, the zone structure of the substance was calculated using density functional theory with the exchange-correlation interaction HSE06. Figure 11 shows the electron density distribution of $NaScB_2O_5$. The valence band ceiling is occupied mainly by O-2p orbitals. The bottom of the conduction band consists mainly of 4d-orbitals of scandium. The width of the forbidden zone is approximately 6 eV.

4. Conclusions

Sodium scandium double borate ($NaScB_2O_5$) was obtained by solid-phase synthesis. The

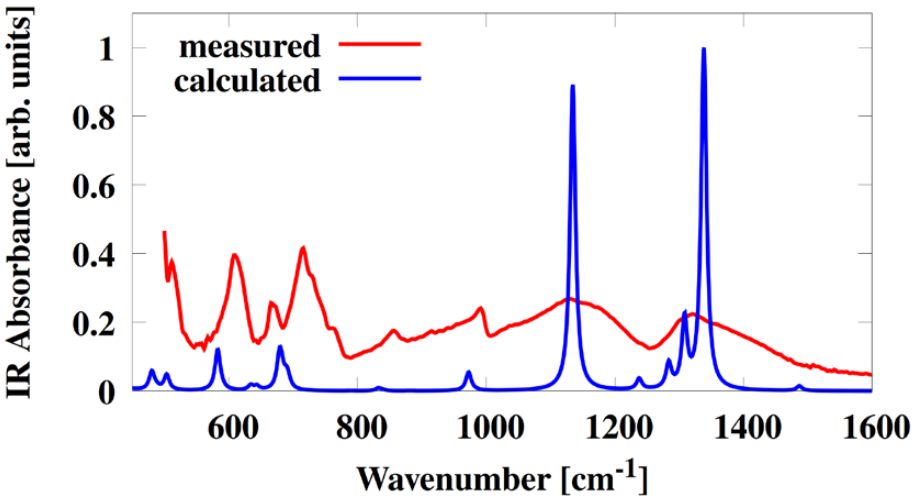

Fig. 10. Measured and calculated infrared spectra of $NaScB_2O_5$

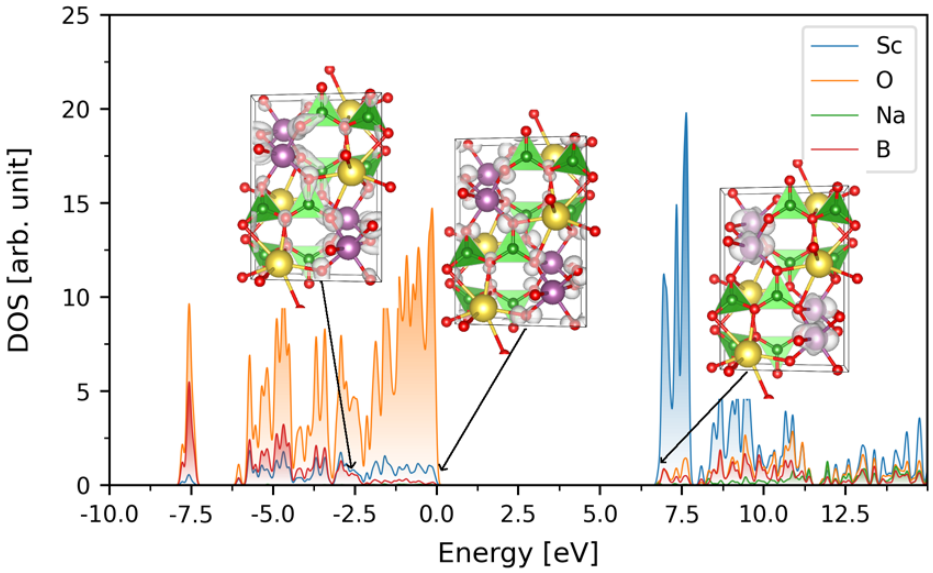

Fig. 11. The total and partial density of states in $NaScB_2O_5$

crystallographic parameters of the synthesized sample were refined using the Rietveld method. The incongruent melting temperature was 1090 °C. A comparison of the experimental and calculated IR spectra showed good agreement of the peak positions, which allowed us to interpret the nature of the vibrations. The valence force sum maps, the energy barriers, and ionic transport pathways of sodium and oxygen ions were calculated, according to which the three-dimensional oxygen conductivity (0.998 eV) and the two-dimensional sodium conductivity (0.936 eV) are considered to be the most probable. The experimental conductivity measurements agree with the calculated data (*E*a = 0.9 eV). The ionic conductivity value of $NaScB_2O_5$ is $0.6 \cdot 10^{-3}$ S /cm at 750 °C. The band gap is 6.83 eV.

Supplementary materials to the article are published in the electronic version on the journal's website.

Contribution of the authors

Andrey N. Sobolev A. – Visualization, Investigation, Writing. Evgeniy V. Kovtunets – Conceptualization, Software. Tatyana S. Spiridonova – Visualization, Investigation, Writing. Alexander I. Bogdanov – Visualization, Investigation, Writing. Alexey K. Subanakov – Data curation, Writing- Original draft preparation, Writing- Reviewing and Editing, Supervision.

Conflict of interests

The authors declare that they have no known competing financial interests or personal relationships that could have influenced the work reported in this paper.

References

1. Huang C., Mutailipu M., Zhang F., ... Pan S. Expanding the chemistry of borates with functional $[BO_2]^-$ anions. *Nature Communications*. 2021;12: 1–8. https://doi.org/10.1038/s41467-021-22835-4

2. Li S., Li W., Li X., ... Li C. A bifunctional primitive strategy induces enhancements of large second harmonic generation and wide UV transmittance in rare-earth borates containing $[B_5O_{10}]$ groups. *Chemical Science*. 2024;15: 8959–8965. https://doi.org/10.1039/d4sc01853b

3. Wu H., Wei Z., Hu Z., Wang J., Wu Y., Yu H. Assembly of π-conjugated $[B_3O_6]$ units by mer-isomer $[YO_5F_3]$ octahedra to design a UV nonlinear optical material, $Cs_2Yb_3O_6F_2$. *Angewandte Chemie*. 2024;136. https://doi.org/10.1002/ange.202406318

4. Zhang W., Hou X., Han S., Pan S. Toward the ultraviolet (UV) or deep-UV nonlinear optical crystals: the combination of π-conjugated planar $[XY_3]$ and tetrahedral $[XY_4]$. *Coordination Chemistry Reviews*. 2024;505: 215664. https://doi.org/10.1016/j.ccr.2024.215664

5. Li Q.-F., Chen W.-F., Lan Y.-Z., Cheng J.-W. Recent progress in ultraviolet and deep-ultraviolet nonlinear optical aluminoborates. *Chinese Journal of Structural Chemistry*. 2023;42(3): 100036. https://doi.org/10.1016/j.cjsc.2023.100036

6. Kang L., Lin Z. Deep-ultraviolet nonlinear optical crystals: concept development and materials discovery. *Light: Science & Applications*. 2022;11: 1–12. https://doi.org/10.1038/s41377-022-00899-1

7. Halasyamani P. S Zhang W. Viewpoint: inorganic materials for UV and deep-UV nonlinear-optical applications.

Inorganic Chemistry. 2017;56: 12077–12085. https://doi.org/10.1021/acs.inorgchem.7b02184

8. Chen C., Li R. The anionic group theory of the nonlinear optical effect and its applications in the development of new high-quality nlo crystals in the borate series. *International Reviews in Physical Chemistry*. 1988;8: 65–91. https://doi.org/10.1080/01442358909353223

9. Chen C., Wu Y., Jiang A., …. Lin S. New nonlinear-optical crystal: LiB_3O_5. *Journal of the Optical Society of America B*. 1989;6(4): 616. https://doi.org/10.1364/josab.6.000616

10. Mori Y., Kuroda I., Nakajima S., Sasaki T., Nakai S. New nonlinear optical crystal: cesium lithium borate. *Applied Physics Letters*. 1995;67: 1818–1820. https://doi.org/10.1063/1.115413

11. Chen C. T., Wang G. L., Wang X. Y., Xu Z. Y. Deep-UV nonlinear optical crystal $KBe_2BO_3F_2$-discovery, growth, optical properties and applications. *Applied Physics B*. 2009;97: 9–25. https://doi.org/10.1007/s00340-009-3554-4

12. Chen C., Wang Y., Wu B., Wu K., Zeng W., Yu L. Design and synthesis of an ultraviolet-transparent nonlinear optical crystal $Sr_2Be_2B_2O_7$. *Nature*. 1995;373: 322–324. https://doi.org/10.1038/373322a0

13. Fröhlich R., Bohatý L., Liebertz J. *Acta Crystallographica Section C: Structural Chemistry*. Die Kristallstruktur von Wismutborat, BiB_3O_6. 1984;40: 343–344. https://doi.org/10.1107/S0108270184004078

14. Guoqing Z., Jun X., Xingda C., …. Fuxi G. Growth and spectrum of a novel birefringent α-BaB_2O_4 crystal. *Journal of Crystal Growth*. 1998;191(3): 517–519. https://doi.org/10.1016/S0022-0248(98)00162-6

15. Zhang S., Wu X., Song Y., Ni D., Hu B., Zhou T. Growth of birefringent $Ca_3(BO_3)_2$ crystals by the Czochralski method. *Journal of Crystal Growth*. 2003;252: 246–250. https://doi.org/10.1016/S0022-0248(03)00867-4

16. Ming H., Xiaolong C., Yuping S., Jun L., Jingtai Z., Chengjun D. $YBa_3B_9O_{18}$: a promising scintillation crystal. *Crystal Growth and Design*. 2007;7(2): 199–201. https://doi.org/10.1021/cg0606141

17. Chen X., Zhang B., Zhang F., …. Pan S. Designing an excellent deep-ultraviolet birefringent material for light polarization. *Journal of the American Chemical Society*. 2018;140: 16311–16319. https://doi.org/10.1021/JACS.8B10009

18. Berger S. V., Hassel O., Webb M., Rottenberg M. The crystal structure of cobaltpyroborate. *Acta Chemica Scandinavica*. 1950;4: 1054–1065. https://doi.org/10.3891/ACTA.CHEM.SCAND.04-1054

19. Cheng W. D., Zhang H., Zheng F. K., Chen J. T., Zhang Q. E., Pandey R. Electronic structures and linear optics of $A_2B_2O_5$ (A = Mg, Ca, Sr) pyroborates. *Chemistry of Materials*. 2000;12: 3591–3594. https://doi.org/10.1021/cm000188l

20. Zhou C., Cheng J., Li H., Beysen S. $Li_{3.366}Mg_{0.317}B_2O_5$: the first pyroborate in the Li_2O-MgO-B_2O_3 system. *Inorganic Chemistry Communications*. 2018;93: 92–96. https://doi.org/10.1016/j.inoche.2018.05.018

21. Maschmeyer E. M., Sanjeewa L. D., Ranmohotti G. S. Crystal structure of $BaMnB_2O_5$ containing structurally isolated manganese oxide sheets. *Acta Crystallogr Sect E Crystallogr Commun*. 2016;72: 1315–11320. https://doi.org/10.1107/S2056989016013074

22. Platunov M. S., Ivanova N. B., Kazak N. V., Ovchinnikov S. G. Crystal structure and magnetism of $Co_{2-x}Ni_xB_2O_5$ pyroborate. *Journal of Siberian Federal University. Mathematics & Physics*. 2011;4: 298–307. Режим доступа: https://elib.sfu-kras.ru/bitstream/handle/2311/2425/platunov.pdf?sequence=1

23. Busche S., Bluhm K. Synthese und Kristallstruktur der ersten zinkhaltigen Pyroborate $Ni_{1.5}Zn_{0.5}(B_2O_5)$ und $Co_{1.5}Zn_{0.5}(B_2O_5)$. *Zeitschrift für Naturforschung B*. 1995;50(10): 1445–1449. https://doi.org/10.1515/znb-1995-1003

24. Yan J., Chu D., Chen Z., Han J. $Li_2PbB_2O_5$: a pyroborate with large birefringence induced by the synergistic effect of stereochemical active lone pair cations and π-conjugated $[B_2O_5]$ groups. *Inorganic Chemistry*. 2022;61(46): 18795–801. https://doi.org/10.1021/acs.inorgchem.2c03469

25. Held P., Becker P. Dipraseodymium(III) pyroborate molybdate(VI), $Pr_2(B_2O_5)(MoO_4)$. *Crystallographic Communications*. 2008;64(6). https://doi.org/10.1107/S1600536808010386

26. Zhang M., An D., Hu C., Chen X., Yang Z., Pan S. Rational design via synergistic combination leads to an outstanding deep-ultraviolet birefringent $Li_2Na_2B_2O_5$ material with an unvalued B_2O_5 functional gene. *Journal of the American Chemical Society*. 2019;141: 3258–3264. https://doi.org/10.1021/jacs.8b13402

27. Becker P., Held P. Crystal structure of sodium scandium borate, $NaScB_2O_5$. *Zeitschrift für Kristallographie – New Crystal Structures*. 2001;216(1-4): 35. https://doi.org/10.1524/NCRS.2001.216.14.35

28. Rietveld H. M. A profile refinement method for nuclear and magnetic structures. *Journal of Applied Crystallography*. 1969;2: 65–71. https://doi.org/10.1107/s0021889869006558

29. Coelho A. A. Topas: general profile and structure analysis software for powder diffraction data. Bruker AXS, 2005.

30. Dinnebier R. E., Leineweber A., Evans J. Rietveld refinement practical powder diffraction pattern analysis using TOPAS. 2019. https://doi.org/10.1515/9783110461381-201

31. Chen H., Wong L. L., Adams S. SoftBV – a software tool for screening the materials genome of inorganic fast ion conductors. *Acta Crystallographica Section B Structural Science, Crystal Engineering and Materials*. 2019;75: 18–33. https://doi.org/10.1107/S2052520618015718

32. Kresse G. Ab initio molecular dynamics for liquid metals. *Journal of Non-Crystalline Solids*. 1995;192–193: 222–229. https://doi.org/10.1016/0022-3093(95)00355-X

33. Perdew J. P., Ruzsinszky A., Csonka G. I., … Burke K. Restoring the density-gradient expansion for exchange in solids and surfaces. *Physical Review Letter.s* 2008;100: 1–4. https://doi.org/10.1103/PhysRevLett.100.136406

34. Togo A., Tanaka I. First principles phonon calculations in materials science. *Scripta Materialia*. 2015;108: 1–5. https://doi.org/10.1016/j.scriptamat.2015.07.021

35. Krukau A. V., Vydrov O. A., Izmaylov A. F., Scuseria G. E. Influence of the exchange screening parameter on the performance of screened hybrid functionals. *The Journal of Chemical Physics*. 2006;125(22). https://doi.org/10.1063/1.2404663

36. Shendrik R. Yu., Plechov P. Yu., Smirnov S. Z. ArDI – the system of mineral vibrational spectroscopy data processing and analysis. *New Data on Minerals*. 2024;58(2): 26–35. (In Russ.). https://doi.org/10.25993/fm.2024.58.2024.008

Information about the authors

Andrey N. Sobolev, Laborant at the Institute of Natural Sciences, Banzarov Buryat State University (Ulan-Ude, Russian Federation).
https://orcid.org/0009-0006-2286-1380
sobolevan02@mail.ru

Evgeniy V. Kovtunets, Research Scientist of the Baikal Institute of Nature Management SB RAS, (Ulan-Ude, Russian Federation).
https://orcid.org/0000-0003-1301-1983
kovtunets@gmail.com

Tatyana S. Spiridonova, Cand. Sci. (Chem.), Senior Research Scientist of the Baikal Institute of Nature Management SB RAS, (Ulan-Ude, Russian Federation).
https://orcid.org/0000-0001-7498-5103
spiridonova-25@mail.ru

Alexander I. Bogdanov, Cand. Sci. (Phys.–Math.), Senior Research Scientist of the Vinogradov Institute of Geochemistry SB RAS, (Irkutsk, Russian Federation).
https://orcid.org/0000-0001-8639-4730
alex.bogdanov2012@gmail.com

Alexey K. Subanakov, Cand. Sci. (Chem.), Head of the Oxide Systems Laboratory of the Baikal Institute of Nature Management SB RAS, (Ulan-Ude, Russian Federation).
https://orcid.org/0000-0002-1674-283X
subanakov@binm.bscnet.ru

Received 24.10.2024; approved after reviewing 02.12.2024; accepted for publication 05.12.2024; published online 25.09.2025.